1

Cation and buffer specific effects on the DNA-lipid interaction

Monica Mura,[1,2,3] Ben Humphreys,[1] Jennifer Gilbert, [1] Andrea Salis,[2,3,]* Tommy Nylander[1,]*

[1]Department of Chemistry, Lund University, P.O. Box 124, SE-221 00 Lund, Sweden.

[2]Department of Chemical and Geological Sciences, University of Cagliari, Cittadella Universitaria, SS 554 bivio Sestu, 09042 Monserrato (CA) (Italy).

[3]Consorzio Interuniversitario per lo Sviluppo dei Sistemi a Grande Interfase (CSGI), Via della Lastruccia 3, Sesto Fiorentino (FI), I-50019 (Italy).

Corresponding Authors

*email: tommy.nylander@fkem1.lu.se (TN); asalis@unica.it (AS)

Statistical summary

4256 words

6 Figures

1 Table

ABSTRACT

Knowledge of DNA - lipids layer interactions is key for the development of biosensors, synthetic nanopores, scaffolds, and gene-carries. These interactions are strongly affected ionic composition of the solvent. We have combined quartz crystal microbalance (QCM) and ellipsometry measurements to reveal how pH buffers and alkaline metal chloride salts affect the interaction of DNA with lipid bilayers (DOTAP/DOPC 30:70 in moles). We found that thickness of the DNA layer adsorbed onto the lipid bilayer decreased in the order citrate > phosphate > Tris > HEPES. The effect of cations does not follow the Hofmeister series ($Li^+ > Na^+ > K^+ > Cs^+$), but thickness of the DNA layer decreases in the order ($K^+ > Na^+ > Cs^+ \sim Li^+$), which was also modulated by the specific buffer effect. The apparent bell-shaped effect of the cation specificity as a function of the Hofmeister series was rationalized by the simultaneous action of two mechanisms namely, the water affinity and the ion dispersion forces effect. DNA-lipid bilayer interactions, judging from the increase in layer thickness are maximal for KCl (100 mM) and citrate buffer (50 mM, pH 7.4) are used.

GRAPHICAL ABSTRACT
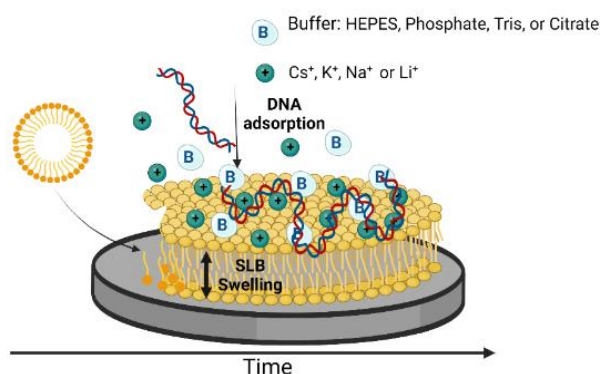
KEYWORDS: DNA-lipid interactions; Hofmeister series; specific buffer effects; biointerfaces; QCM-D; Ellipsometry.

1. INTRODUCTION

Ion specificity was discovered by Hofmeister in 1888 while studying salt-induced egg white protein precipitation/solubilization [1]. Since then, specific ion (Hofmeister) phenomena have been found in a myriad of bio-systems [2] including enzymes [3–6], proteins [7–9], lipids [10], and nucleotides [11–14]. To date, specific ion effects on biological systems are not fully understood [2,15–17]. In such systems, hydrogen ion concentration, commonly expressed in terms of pH (=−log a_{H+}), strongly affects biomolecules' structure and function. For these reasons, pH must be strictly controlled by mean of buffers (a weak acid/base in the presence of its conjugated base/acid). The buffer concentration is generally low with respect to other salts, so that their possible specific effects are often neglected. However, in a pioneering work, Ninham and co-workers showed that the catalytic activity of restriction enzymes was both ion and buffer specific [18]. Buffers changed the ion sequence (Hofmeister series) by which they affect the enzymatic activities if cacodylate instead of phosphate buffer regulated the pH [18]. Similar observations were made in other systems as, for example, pH measurements [19] or the electrophoretic mobility of lysozyme [20]. More recently, "specific buffer effects" have been investigated in more detail and new interesting results have emerged [21–29]. All these findings put serious doubts on the validity and predictive capacity of the basic theories of strong (Debye-Hückel) and weak (Henderson-Hasselbalch) electrolytes [30].

Phospholipids are the main constituent of biological membranes and have also been found to be interesting model systems to investigate specific ion effects [31]. The surface pressure, the area per lipid molecule, and the water layer spacing in stacks of lipid bilayers were found to be specifically influenced by ions type and concentration [32]. The influence of buffers on lipid bilayers is often ignored, in spite of the fact that e.g. membrane bending elasticity, investigated through electroswelling and phase contrast microscopy, was found to be specifically affected by buffers (HEPES, MES, BES, MOPS, PIPES, Tris and histidine) [33,34]. Buffers having zwitterionic form

(HEPES and histidine) had a smaller effect than cationic buffers (MES, MOPS, Tris), which gave a higher decrease of the bending rigidity [34].

Lipids mixtures of cationic methyl N-[1-(2,3-dioleilooksy)-propyl]-N,N,N-trimethylammonium chloride (DOTAP) and zwitterionic dioleylphosphatidylcholine (DOPC) have been used for biomedical applications involving DNA/RNA interactions [35]. Including DNA in lipid structures has driven to new applications, like biosensors [36], synthetic nanopores [37], scaffolds [38], and nucleic acid carriers [39–43] for gene therapy [44]. Zwitterionic membranes becomes positively charged in the presence of (multivalent) cations. This facilitate the adsorption of negatively charged DNA biomolecules [45–47]. The role of monovalent cations in this respect have so far not been as extensively studied compared to divalent cations [48]. For example, the interaction of phospholipid monolayers with DNA was found to be stronger with calcium than with magnesium and barium [49].

Quartz crystal microbalance with dissipation monitoring (QCM-D) and ellipsometry are powerful techniques to investigate lipid bilayer formation and DNA adsorption in real time [50,51]. QCM-D was used to investigate the formation of DOPC lipid bilayer and monovalent cation specific effects and it was found that the thickness increased in the order $Cs^+ < K^+ < Na^+ < Li^+$ in Tris buffer pH 7.4 [52]. Ellipsometry is a useful complementary technique as it allows the quantification of the adsorbed dry mass of biomolecules [53].

Specific ion effects are commonly studied neglecting the superimposing specific buffer effects. In this work the specific effects of buffers and cations on DNA-lipid bilayer interactions were both studied through QCM-D and ellipsometry. Specifically, we investigated how specific buffer and cations effects affect the adsorption of DNA on DOTAP/DOPC lipid bilayers on a silica surface (Scheme 1). To this purpose, four different buffers (citrate, phosphate, Tris, and HEPES) at the same pH (= 7.4) also containing different (Li^+, Na^+, K^+, and Cs^+) chloride salts were used. To date, the combined specific buffer and cation effect on lipid/DNA interactions has seldom been investigated.

5

Its understanding is important to shed light on the combined specific cation/buffer effect as well as for biomedical applications like for gene delivery formulations [54,55].
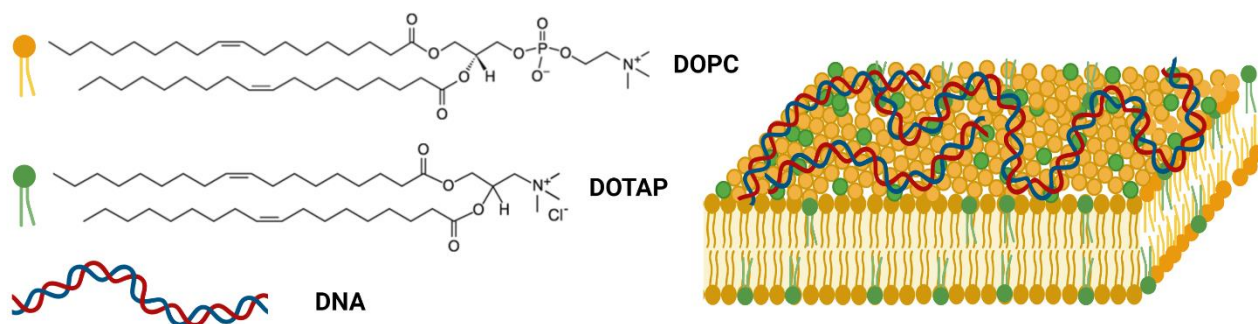
Scheme 1. Interactions of DNA with a lipid bilayer formed by DOTAP/DOPC.

2. EXPERIMENTAL SECTION

2.1 Materials

 N-[1-(2,3-dioleilooksy)-propyl]-N,N,N-trimethylammonium chloride (DOTAP, 99.5%) and dioleoylphosphatidylcholine (DOPC, 99.7%) were purchased from Avanti Polar Lipid. Calf thymus DNA stock solution 9-12 mg mL^{-1}, Tris(hydroxymethyl)aminomethane hydrochloride (Tris, 99.9%), sodium citrate tribasic dihydrate (99%), monobasic sodium phosphate monohydrate (99%), disodium hydrogen phosphate anhydrous (99%), potassium phosphate monobasic (99%), HEPES (100%), hydrochloric acid (37%), sodium hydroxide (97%), lithium chloride (99%), sodium chloride (99.9%), potassium chloride (99%), and caesium chloride (99.9%) were purchased from Sigma Aldrich. Disodium hydrogen phosphate anhydrous (99%), citric acid monohydrate (99%), were purchased from VWR Chemicals. Solutions were prepared with a concentration of 0.050 M buffer (HEPES, citrate, phosphate, Tris) and pH was adjusted to 7.4. Buffer-salt solutions were prepared adding monovalent (Li, Na, K, Cs) chloride salt to a concentration of 0.1 M. Phosphate buffer saline (PBS; pH 7.2) solution consisted of sodium chloride (0.155 M), sodium phosphate dibasic (0.003 M) and potassium phosphate monobasic (0.001 M).

2.2 Sample preparation

Lipids stock solutions were prepared by dissolving DOTAP or DOPC in chloroform to a final concentration of 10 mg mL^{-1} each and stored at -22 °C before use. 70 µL of DOTAP and 180 µL of DOPC stock solutions was then mixed in a vial to obtain a DOTAP/DOPC molar ratio of 30:70. Chloroform was evaporated under a flow of nitrogen; thus a 2.5 mg film of dried lipids was obtained. Liposomes solution was prepared by adding 5 mL PBS to 2.5 mg of the dried lipid film and by mixed through a vortex. The coarse dispersion was then sonicated using a tip sonicator Vibra-Cell VCX 130 (Sonics & Materials Inc., Newton, CT, USA) with the following settings: 15 mins sonication time, 10s on, 10s off, 50% amplitude until it appeared clear. Typical 80/20 DOPC/DOTAP vesicles have a hydrodynamic diameter of ~30 nm as determined by DLS measurements [56]. The vesicular dispersion was diluted in a 1:3 ratio with PBS to prepare the supported bilayer by means of vesicle fusion. DNA solution was diluted without further purification in the appropriate buffer and buffer-salt solutions until the final concentration of 50 µg mL^{-1}.

2.3 Quartz crystal microbalance with dissipation monitoring (QCM-D)

QCM-D is an acoustic surface-sensitive technique which provides simultaneous, real-time information about the mass and viscoelastic properties of thin films adsorbed on a quartz crystal sensor [57]. The sensor in our case was functionalised by a sputtered film of silica. The mass per area unit (Δm) of the adsorbed layer can be quantified from the shift in the resonance frequency (Δf) of the sensor. Viscoelastic properties are determined from the dissipation energy D or damping of the oscillation. Increasing the mass of an adsorbed layer on the sensor decreases the resonance frequency of the crystal and, for a rigid compact film, no dissipation occurs. Δm (mg m^{-2}) is hence related to Δf (Hz) through the Sauerbrey equation:

$$\Delta m = \frac{C}{n} \Delta f \tag{1}$$

Where, C (≈ 17.7 ng Hz^{-1} cm^{-2}) is the mass sensitivity constant related to the properties of quartz for a 5 MHz crystal, and n is the number of harmonic (1, 3, 5, 7, ...). From adsorbed mass, it is possible to calculate the layer thickness d (nm) knowing the density ρ (1.1 g cm^3) [58], according to: [57]

$$d = \frac{\Delta m}{\rho} \tag{2}$$

For a viscous or a viscoelastic film, the dissipation also increases. Larger differences between overtones correspond to a more viscous film. The thickness and adsorbed amount can also be calculated under these conditions, however this requires a more complex model like the Voigt model [59]. Here, Δf and ΔD are respectively the imaginary and real parts of the β-function:

$$\Delta f = Im(\frac{\beta}{2\pi\rho_0 h_0}) \quad \text{and} \quad \Delta D = -Re(\frac{\beta}{\pi f \rho_0 h_0}) \tag{3}$$

Where $\beta = \kappa_1 \xi_1 (\frac{1-Ae^{2\xi_1 h_1}}{1-Ae^{2\xi_1 h_1}})$ is related to the thickness h of the quartz plate (0) and layer adsorbed (1); ξ is associated to the shear stress at the interface and the elastic shear modulus [59].

QCM-D measurements were performed using a Q Sense E4 system from Q Sense (Lund, Sweden) with four measurement cells, each equipped with a silica sensor from Biolin Scientific Q Sense. Silica covered sensors were first cleaned in 2% Helmanex solution, rinsed with MilliQ water, ethanol 99.5% for 10 minutes in a ultrasounds bath, dried under a nitrogen flow, and treated in a plasma cleaner from Harrick Scientific (New York, USA) for 10 min. Silica sensors were placed in the flow cells. The flow of liquid through the QCM modules was controlled by means of an external peristaltic pump (Ismatec IPC-N 4) to assure constant flow throughout the experiment. Before each measurement, the sensors were allowed to equilibrate in water until a stable baseline was reached (30 min). The experiments were carried by flowing through the following solutions: i. buffer solution to equilibrate the sensors (30 min), ii. liposomes in PBS (30 min), iii. Buffer (HEPES, Tris, citrate, phosphate) rinsing to remove PBS and liposomes (30 min); iv. DNA in buffer solution (150 min) and v. buffer rinse (60 min). Data were analyzed with Eq. 1 and Eq 2 through MatLab R2022b software.

2.4 Ellipsometry

Ellipsometry is an optical surface sensitive technique, which measures changes in the state of polarized light upon reflection. From measurements of the relative amplitude shift, Psi (ψ) and phase

change, Delta (Δ), of the two component light waves of the (elliptically) polarized light, we can obtain the refractive index and thickness of a thin film. A Rudolph Research ellipsometer (type 43603-200E) equipped with a xenon arc lamp was used to characterize the lipid bilayer formation and the subsequent adsorption of DNA in each of the buffers or buffer-salt solution following the same procedure adopted for the QCM-D measurements. All measurements were performed at a wavelength, $\lambda = 4015$ Å and an incidence angle of 68.00°. The silicon substrates were placed inside a thermostatic (25 °C) trapezoid 5 mL cuvette equipped with a magnetic stirrer. Solutions were fluxed into the cell with a peristaltic pump. The thickness of the adsorbed layers was characterized by recording the ellipsometry angles ψ and Δ, with a time resolution of a few seconds and analysed through VWASE32 software [60]. The multilayer model used here consisted of sequentially: a silicon layer, a silica layer, a mixed layer of water and lipid with a certain thickness and refractive index. The properties of the lipid layer was evaluated before the mixed layer of DNA and solvent. The linear effective medium approximation (EMA) was used to interpolating the dielectric properties for the layer from its components. This will give an ensemble solvated film thickness average over the size of the measurement spot. [60] For ellipsometry modelling, the real (n) and imaginary (k) components of the refractive indices of each material used were: silicon, $n = 4.15$, $k = 0.0439$, silica, $n = 1.461$, $k = 0$, SLB, $n = 1.48$, $k = 0$, DNA, $n = 1.616$, $k = 0$, and water, $n = 1.335$ and $k = 0.5$. The n and k values for water were employed for all electrolyte solutions; at the highest electrolyte concentration there was minimal difference in the refractive index of the solution or the fitted layer thickness.

3. RESULTS

The formed supported lipid bilayer (SLB) with a DOTAP/DOPC molar ratio of 30:70 was investigated by QCM-D. DNA, dissolved in different buffer/salt solutions, was then flowed through the cell to monitor the adsorption on the SLB depending on the buffer and salt composition. Fig. 1 shows the frequency shift (Δf) and the dissipation energy shift (ΔD) of the 7th overtone respect to the

solvent during the SLB formation and DNA adsorption in 50 mM buffer (HEPES, Tris, phosphate, and citrate) solutions at pH = 7.4.
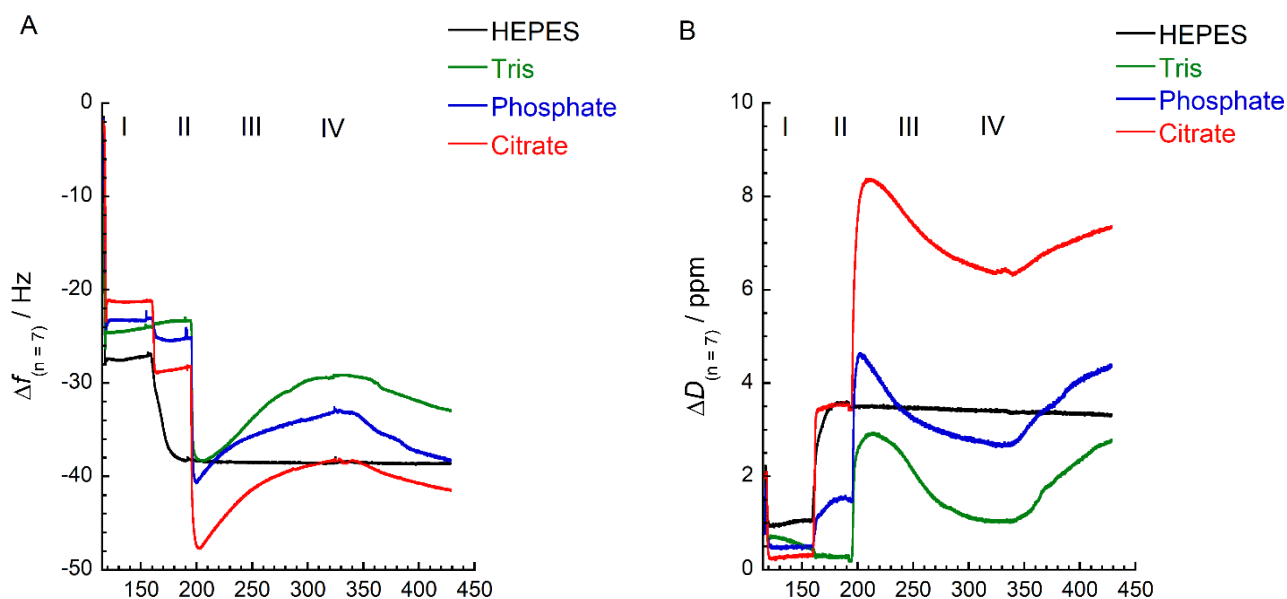

Fig. 1. Frequency shift, Δf (**A**) and Dissipation energy, ΔD (**B**) for the 7th overtone recorded during the SLB formation, using QCM-D. Measures are carried in parallel in each cell using HEPES (black line), citrate (red line), phosphate (blue line) and Tris (green line) 50 mM buffer solution. Initially the sensor equilibration in MilliQ water, baseline acquisition of PBS and reference buffer was performed. Step I: injection of vesicles to form the SLB in PBS; Step II: rinsing with the different buffer solutions; Step III: injection of the DNA solution; Step IV: rinsing with buffer.

The bilayers were deposited on the silica sensor surface which is slightly negatively charged at physiological pH 7.4 [61] (Fig. 1 step I). The average frequency for deposited bilayers in PBS resulted of Δf = -24 ± 2 Hz, whereas only a minor change in dissipation energy ΔD = 0.6 ± 0.3 ppm was observed. The cells were rinsed with the different buffer solutions (step II) and the DNA in the corresponding buffer solution was then introduced (step III). In HEPES buffer (black line), no change was observed after DNA addition (step III), which suggests that DNA was not adsorbed onto the SLB. In Tris, phosphate, and citrate buffers the sudden decrease of Δf and increase of ΔD is associated to DNA adsorption (step III). Interestingly, this is followed by a slow increase of Δf and decrease of D. The former can be interpreted as a slow release of water, which is consistent with the decrease in D that suggests a reorganisation into a more compact layer until the equilibrium is reached (step IV). The final rinsing causes small decrease in Δf and corresponding increase of D, indicating a slight

10

swelling of the layer. The small change in D during the SLB formation and large increasing during the DNA adsorption indicates two differences in the properties of the formed layers, i.e., a rigid lipid bilayer and a viscoelastic DNA extended layer. Planar SLBs constitute a model system where it is possible to apply Sauerbrey equation (Eq. 1). Indeed, a planar SLB is commonly considered a thin, acoustically rigid and uniform film, having a negligible amount of trapped water into the structure [53]. SLB adsorbed amount (Δm) could therefore be calculated from the frequency shift using the Sauerbrey equation and thickness (d) from Eq. 2 [57] obtaining $\Delta m = 4.8 \pm 0.6$ mg m^{-2}, and $d = 4.0 \pm 0.5$ nm, respectively. The samples with SLBs were then rinsed with the different 50 mM buffers (HEPES, citrate, phosphate, and Tris) and 100 mM buffer-salt solutions (Cs$^+$, K$^+$, Na$^+$, Li$^+$ chlorides). Apart for HEPES with no added salt, the amount of lipid bilayer (with any amount of entrapped water) was not significantly affected neither by the different cations (Fig. 2A and S1A) nor by buffers (Fig. 2B and S1B) (Supporting information file).
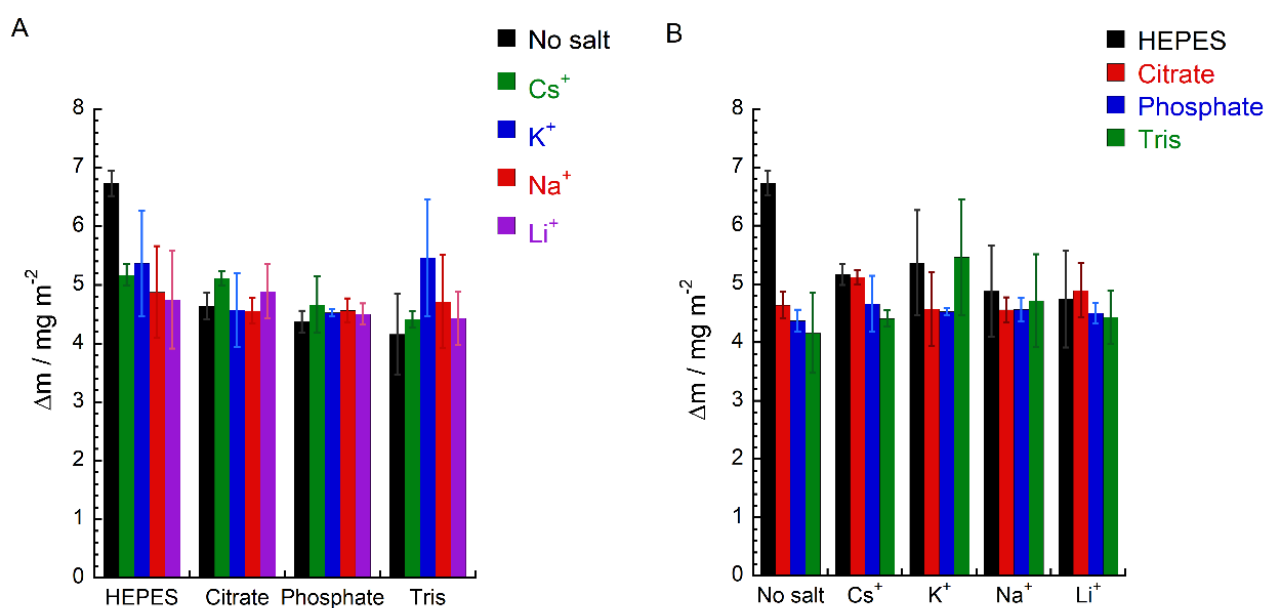

Fig. 2. QCM-D measurements on lipid bilayer adsorption. Cations (**A**) and buffers (**B**) effects on adsorbed amount (Δm) of SLB in 50 mM HEPES, citrate, phosphate and Tris buffer solutions with 100 mM chloride salts (Cs$^+$, K$^+$, Na$^+$, Li$^+$ 100 mM). Adsorbed amount (Δm) was calculated with Eq. 1.

Different buffer/salt solutions containing 50 μg mL^{-1} of DNA were sequentially flowed through the sample cells until a plateau in frequency and dissipation was observed, indicating the reaching of the equilibrium. Since the DNA layer has viscoelastic properties, the Voigt model [62] was used to analyse the data using the previously formed SLB after equilibration with buffers as a reference to disentangle DNA contribution only.
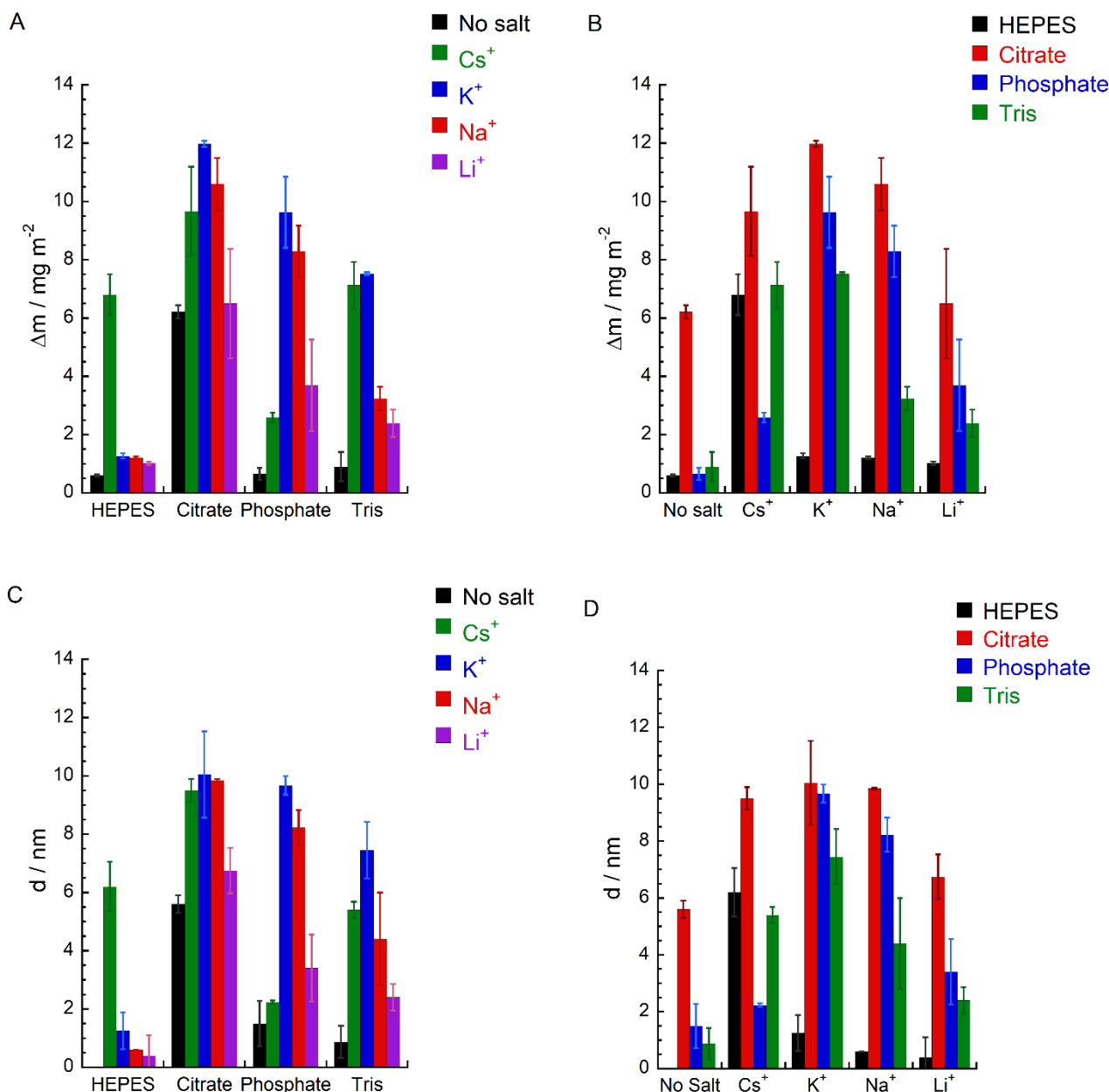

Fig. 3. QCM-D measurements on DNA adsorption on the lipid bilayer determined through Voigt model (Eq.3) by Qsense Dfind software. Specific cation and buffer effects of 100 mM chloride salts (Cs$^+$, K$^+$, Na$^+$, Li$^+$ 100 mM) in 50 mM HEPES, citrate, phosphate and Tris buffer solutions on adsorbed amount (**A** and **B**) and thickness (**C** and **D**) on the adsorbed layer.

Fig. 3A shows DNA adsorbed amount as a function of cations in different buffer solutions. Compared with the other buffers, DNA adsorption on SLBs in the presence of HEPES is low for all added salts (KCl, NaCl, and LiCl), except for CsCl, which promoted a strong adsorption of DNA on the SLBs (Fig. 3A). The adsorbed amount of DNA in citrate, phosphate and Tris buffers followed a "bell-shaped" cation specific sequence with KCl giving the highest adsorbed amount of DNA on the SLB (Fig. 3A). Fig. 3C showed thickness increase due to the adsorption of a DNA layer on SLB, which depends on the type of cation. The results follow the trend observed for the adsorbed amount (Fig. 3A). Plotting the adsorbed amount (Fig. 3B) and thickness (Fig. 3D) of DNA layer as a function of buffer type, highlights the following buffer specific trend: citrate > phosphate > Tris > HEPES for LiCl, NaCl, and KCl salts. The addition of CsCl, instead, promoted a different trend: citrate > Tris ~ HEPES > phosphate. With no added salts, the adsorbed amount and thickness followed the order: citrate >> phosphate ~ HEPES > Tris (Fig. 3B-D).

The same systems investigated above were then analysed with ellipsometry. The difference between QCM-D and ellipsometry is that the trapped solvent contributes to the mass measured by the former, while the latter can be used to determine the amount of dry matter [63]. Thickness values from QCM-D are generally higher than those measured by ellipsometry [64]. Hence, a combination of the two techniques can provide insights into the solvent content in the adsorbed film and the specific role of electrolytes to favour/disfavour the adsorption [65]. Ellipsometry was thus used as a complementary characterization technique to evaluate if the variation in thickness layer was due to lipid and DNA structures or to the trapped solvent into the SLB film. Fig. S2 shows the thickness of SLB layers and adsorbed DNA obtained by ellipsometry measurements. SLB average thickness measured by ellipsometry is 3.7 ± 0.3 nm (Fig. S2A and Fig. S2B). As expected, it is slightly lower with respect to the value obtained through QCM-D (4.6 ± 0.3 nm). DNA thickness (~ 2 nm) suggests that the main part of the DNA molecules adsorbed are positioned horizontally respect to the SLB

13

(Fig. S2C and S2D) film. Thickness values obtained by ellipsometry measurements did not show a substantial buffer or cation specific trend.

4. DISCUSSION

Usually, specific ion effects studies focus on the single aspect of either strong or weak electrolytes (buffers) influence on the system under consideration. Buffer type is commonly chosen depending on their pK_a according to the Henderson-Hasselbalch equation, without considering buffer specific effects. We have observed that buffer and cation specific effects influenced each other. Our results show the effect cations on adsorbed amount and of thickness of the adsorbed layer of DNA follow a "bell-shaped" effect as a function of the Hofmeister series. Collins explained ion specific effects through the empirical "law of water matching affinities" (LMWA) [66]. It states that cations and anions with similar values of hydration enthalpies (a measure of ion water affinity) form stable ion pairs. Ions with highly negative values of hydration enthalpies are classified as kosmotropes (water structure makers), while those with low negative values of hydration enthalpies are classified a chaotropes (water structure breakers). According to LMWA, the cation interaction with DNA (kosmotropic) phosphate backbones should follow the order: $Li^+ > Na^+ > K^+ > Cs^+$. That is, Li^+, a strong kosmotrope, should interact more effectively with the negatively charged phosphate groups, thus allowing a lower adsorption of DNA on mostly cationic SLBs. Cs^+ should interact less with phosphates thus resulting in a lower DNA adsorption on SLBs. An alternative explanation of ion specificity is due to Ninham's theory of ion dispersion forces [67]. This theory explains the Hofmeister series as the result of ion specific dispersion forces that is determined by ion polarizabilities (α). Polarizability and hydration enthalpy values for each cation are reported in Table 1.

Table 1. Static polarizabilities (α_0) [68] and hydration enthalpies ($\Delta H_{\text{Hydration cation}}$) [69] for alkali cations.

Cation	α_0 / Å^3	$\Delta H_{\text{Hydration}}$ / kJ mol^{-1}
Cs^+	2.354	-264
K^+	0.795	-322
Na^+	0.131	-409
Li^+	0.028	-519

Polarizability is an ion specific electric property ($\alpha_{Cs+} > \alpha_{K+} > \alpha_{Na+} > \alpha_{Li+}$) that follow an opposite cation sequence respect to that predicted by LMWA. However, in citrate, phosphate and Tris buffers, the obtained trends are not monotonically changing in with the order of the Hofmeister series but, rather, a "bell shaped" cationic series (Fig. 3) That is, for example in phosphate buffer, DNA adsorption on SLB decreases in the order $K^+ > Na^+ > Li^+ > Cs^+ > $ no salt. To investigate the molecular origin of the specific cation effect in DNA-SLB interactions, the correlation between the adsorbed amount Δm (and thickness, d) and either the difference in hydration enthalpies ($\Delta H_{\text{hydration anion}} - \Delta H_{\text{hydration cation}}$) or the static polarizabilities of anions and cations (α_0) are shown in Fig. 4A-D. Hydration enthalpies are related to LMWA [66], whereas ion polarizabilities are related to the theory of ion dispersion forces [67].
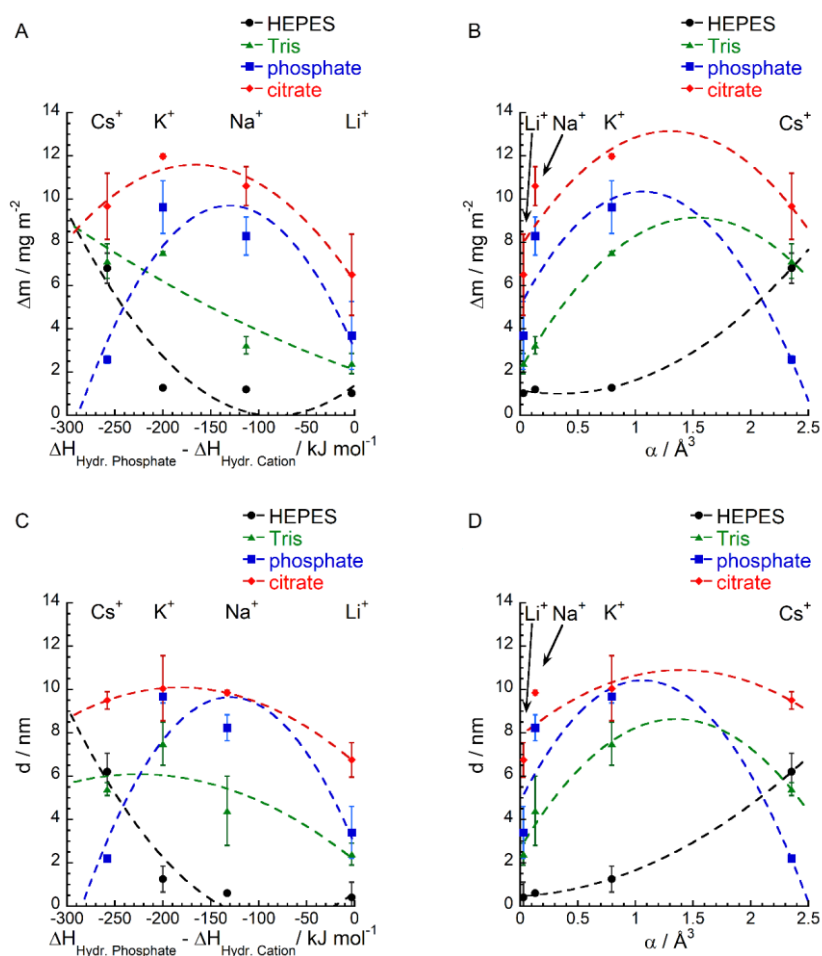
Fig. 4. Effect of cations on DNA adsorbed amount (A and B) and thickness layer (C and D) on SLB vs. hydration enthalpy ($\Delta H_{Hydration}$) and polarizability (α). $\Delta H_{Hydration}$ is reported as difference between hydration enthalpy of phosphate backbones ion ($\Delta H_{Hydration\ Phosphate} = -522$ kJ mol^{-1}) and the hydration enthalpy of cations[69]. The dotted curves are guides for the eye.

Fig. 4A shows a plot of Δm vs the difference in hydration enthalpies ($\Delta H_{hydration}$) of dihydrogen phosphate ion (taken as a reference anionic group due to its similarity with phosphates in DNA surface) and those of the different cations. Fig. 4B shows a plot of Δm vs cation static polarizabilities. Cations show a ''bell-shaped'' trend for both correlations (Fig. 4A and B). If LMWA was the only mechanism at work, the strength of interaction between cations and negatively charged phosphates (classified as kosmotropes) would decrease in going from the kosmotropic lithium to the chaotropic cesium. The order would be reversed if, according to ion dispersion forces theory, polarizability was accounted as the main factor. Since the observed trends do not agree neither with LMWA nor with the polarizability order, the cation specific ''bell-shaped'' order is a clear indication that both mechanisms are at work and operate in opposite directions. Similar sequences were previously

16

observed for Haemoglobin aggregation, BSA Brownian motion [70,71], and enzymatic activities [72]. A recent development of Ninham's theory, devoted to include LMWA in a more complete theory [73–75], was able to reconcile the two apparently different approaches. Scheme 2 shows how specific cation binding on DNA surface modulates its adsorption on SLB as detected by QCM-D measurements.
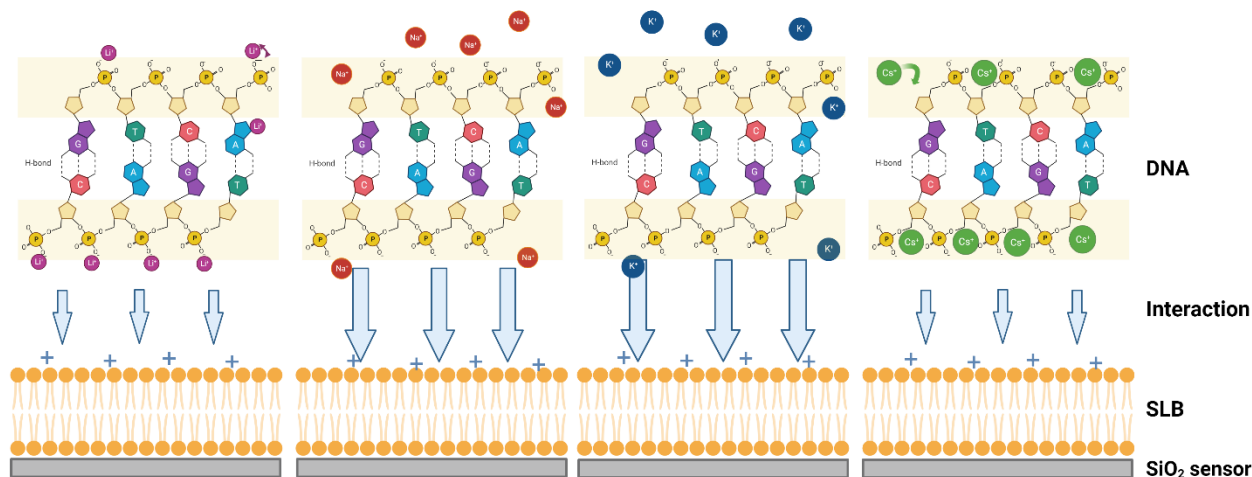
Scheme 2. Specific cation effects on DNA-supported lipid bilayer (SLB) interactions. Small light blue arrows represent a weaker DNA-SLB interaction due to strong adsorption of Li^+ and Cs^+ on the negatively charged DNA phosphate backbones. Big light blue arrows represent a stronger DNA-SLB interaction due to weak adsorption of K^+ and Na^+ on the negatively charged DNA phosphate backbones.

Additionally, Fig. 4 shows that the bell-shaped cation specific trend is also buffer specific. That is, an additional buffer specificity is superimposing that of cations going beyond the simple effect of pH. The experimental trends show a complex interplay between cation and buffer specificity at DNA-SLB charged interface. Negatively charged buffer species (i.e. citrate and phosphate) result in a stronger adsorption of DNA to SLBs. This is confirmed by DLS measurements of diffusion coefficients of DNA in function of temperature in the presence of 10 mM different buffers (Fig. S3). Diffusion coefficients increase linearly with temperature (range 30 – 70 °C) with buffer-specific slopes which follow the trend citrate > phosphate > Tris > HEPES. The series of DNA diffusion coefficients suggest that negatively charged buffer species (e.g. citrate and phosphate) interact with

the negatively charged surface of DNA making it even more negative. From QCM data, with no added salt and in the presence of K^+, Na^+ or Li^+ DNA adsorption follows the specific buffer trend: citrate > phosphate > Tris > HEPES. A similar order was found for the intermolecular interactions among proteins [21], lysozyme adsorption on mesoporous silica [76], and as well with DNA thermal stability [29].

5. CONCLUSIONS

In this work the interplay among buffers at fixed pH and cation specificity on DNA – DOTAP/DOPC supported lipid bilayers was studied. DNA adsorption on SLBs was favoured by the presence of monovalent cations and pH buffer in a specific way. The most effective cations to screen DNA phosphate backbones, Li^+ and Cs^+, result in a lower DNA adsorption on SLB. We hypothesize that screening is driven by the law of matching water affinities [66] for Li^+ and by ion dispersion forces [67] for Cs^+ (Scheme 2). On the contrary, K^+, which lays in the middle of the cation Hofmeister series, screens the charges of phosphate groups on the DNA thus leading to a stronger DNA adsorption on SLBs. The final outcome is a "bell-shaped" effect the cation when following the Hofmeister series. Furthermore, our results show a superimposing buffer effect on DNA-SLB interactions. Driven by their polarizability, trivalent citrate, and divalent phosphate buffer ions, as well as chloride ($Tris^+$ counterion) likely made DNA surface more negative thus favouring the electrostatic attraction with positively charged SLBs. On the contrary, zwitterionic HEPES buffer could not work through this mechanism. In summary, this work goes beyond previous works regarding buffer effects on lipid bilayers [33,34,77] or DNA [29], examining for the first time simultaneous specific cation and buffer effects on DNA-SLB interactions. A suitable choice of strong (KCl) and weak (citrate or phosphate) electrolytes at physiological pH can maximize DNA-SLB interactions. This result could be relevant for gene-delivery formulation and storage. Future work is needed to further investigate and disentangle the specific buffer and cation effect by a theoretical point of view.

Acknowledgements

REFERENCES

[1]   F. Hofmeister, Arbeiten aus dem pharmakologischen Institut der deutschen Universität zu Prag. 12. Zur Lehre von der Wirkung der Salze. Dritte Mittheilung., Arch. Exp. Pathol. Pharmakol. 25 (1888) 1–30.

[2]   P. Lo Nostro, B.W. Ninham, Hofmeister Phenomena: An Update on Ion Specificity in Biology, Chem. Rev. 112 (2012) 2286–2322. https://doi.org/10.1021/cr200271j.

[3]   E. Sedlák, D. Sedláková, J. Marek, J. Hančár, K. Garajová, G. Žoldák, Ion-Specific Protein/Water Interface Determines the Hofmeister Effect on the Kinetic Stability of Glucose Oxidase, J. Phys. Chem. B. 123 (2019) 7965–7973. https://doi.org/10.1021/acs.jpcb.9b05195.

[4]   C. Carucci, A. Salis, E. Magner, Electrolyte effects on enzyme electrochemistry, Curr. Opin. Electrochem. 5 (2017) 158–164. https://doi.org/10.1016/j.coelec.2017.08.011.

[5]   M. Collu, C. Carucci, A. Salis, Specific Anion Effects on Lipase Adsorption and Enzymatic Synthesis of Biodiesel in Nonaqueous Media, Langmuir. 36 (2020) 9465–9471. https://doi.org/10.1021/acs.langmuir.0c01330.

[6]   K. Sakai, Y. Sato, M. Okada, S. Yamaguchi, Enhanced activity and stability of protein-glutaminase by Hofmeister effects, Mol. Catal. 517 (2022) 112054. https://doi.org/10.1016/j.mcat.2021.112054.

[7]   O. Becconi, E. Ahlstrand, A. Salis, R. Friedman, Protein-ion Interactions: Simulations of Bovine Serum Albumin in Physiological Solutions of NaCl, KCl and LiCl, Isr. J. Chem. 57 (2017) 403–412. https://doi.org/10.1002/ijch.201600119.

[8]   T. Pivetta, G. Lusci, C. Carucci, D.F. Parsons, A. Salis, M. Monduzzi, Specific electrolyte effects on hemoglobin in denaturing medium investigated through electro spray ionization mass spectrometry, J. Inorg. Biochem. 234 (2022) 111872. https://doi.org/10.1016/j.jinorgbio.2022.111872.

[9]   G. Lusci, T. Pivetta, C. Carucci, D.F. Parsons, A. Salis, M. Monduzzi, BSA fragmentation specifically induced by added electrolytes: An electrospray ionization mass spectrometry investigation, Colloids Surfaces B Biointerfaces. 218 (2022) 112726. https://doi.org/10.1016/j.colsurfb.2022.112726.

[10]   V. Alfredsson, P. Lo Nostro, B. Ninham, T. Nylander, Morphologies and Structure of Brain Lipid Membrane Dispersions, Front. Cell Dev. Biol. 9 (2021) 1–14. https://doi.org/10.3389/fcell.2021.675140.

[11]   M. Egli, DNA-Cation Interactions, Chem. Biol. 9 (2002) 277–286. https://doi.org/10.1016/S1074-5521(02)00116-3.

[12]   W. Zhou, R. Saran, J. Liu, Metal Sensing by DNA, Chem. Rev. 117 (2017) 8272–8325.

https://doi.org/10.1021/acs.chemrev.7b00063.

[13] B. Gao, X.-M. Hou, Opposite Effects of Potassium Ions on the Thermal Stability of i-Motif DNA in Different Buffer Systems, ACS Omega. 6 (2021) 8976–8985. https://doi.org/10.1021/acsomega.0c06350.

[14] P. Doty, H. Boedtker, J.R. Fresco, R. Haselkorn, M. Litt, Secondary structure in ribonucleic acids, Proc. Natl. Acad. Sci. 45 (1959) 482–499. https://doi.org/10.1073/pnas.45.4.482.

[15] K.P. Gregory, G.R. Elliott, H. Robertson, A. Kumar, E.J. Wanless, G.B. Webber, V.S.J. Craig, G.G. Andersson, A.J. Page, Understanding specific ion effects and the Hofmeister series, Phys. Chem. Chem. Phys. 24 (2022) 12682–12718. https://doi.org/10.1039/d2cp00847e.

[16] P. Jungwirth, P.S. Cremer, Beyond Hofmeister, Nat. Chem. 6 (2014) 261–263. https://doi.org/10.1038/nchem.1899.

[17] A. Salis, B.W. Ninham, Models and mechanisms of Hofmeister effects in electrolyte solutions, and colloid and protein systems revisited, Chem. Soc. Rev. 43 (2014) 7358–7377. https://doi.org/10.1039/C4CS00144C.

[18] H.-K. Kim, E. Tuite, B. Nordén, B.W. Ninham, Co-ion dependence of DNA nuclease activity suggests hydrophobic cavitation as a potential source of activation energy, Eur. Phys. J. E. 4 (2001) 411–417. https://doi.org/10.1007/s101890170096.

[19] A. Salis, M.C. Pinna, D. Bilaničová, M. Monduzzi, P. Lo Nostro, B.W. Ninham, Specific Anion Effects on Glass Electrode pH Measurements of Buffer Solutions: Bulk and Surface Phenomena, J. Phys. Chem. B. 110 (2006) 2949–2956. https://doi.org/10.1021/jp0546296.

[20] F. Cugia, M. Monduzzi, B.W. Ninham, A. Salis, Interplay of ion specificity, pH and buffers: insights from electrophoretic mobility and pH measurements of lysozyme solutions, RSC Adv. 3 (2013) 5882. https://doi.org/10.1039/c3ra00063j.

[21] A. Salis, L. Cappai, C. Carucci, D.F. Parsons, M. Monduzzi, Specific Buffer Effects on the Intermolecular Interactions among Protein Molecules at Physiological pH, J. Phys. Chem. Lett. 11 (2020) 6805–6811. https://doi.org/10.1021/acs.jpclett.0c01900.

[22] P. Pavani, K. Kumar, A. Rani, P. Venkatesu, M.J. Lee, The influence of sodium phosphate buffer on the stability of various proteins: Insights into protein-buffer interactions, J. Mol. Liq. 331 (2021) 115753. https://doi.org/10.1016/j.molliq.2021.115753.

[23] S. Brudar, B. Hribar-Lee, Effect of buffer on protein stability in aqueous solutions: A simple protein aggregation model, J. Phys. Chem. B. 125 (2021) 2504–2512. https://doi.org/10.1021/acs.jpcb.0c10339.

[24] S. Brudar, B. Hribar-Lee, The role of buffers in wild-type hewl amyloid fibril formation mechanism, Biomolecules. 9 (2019). https://doi.org/10.3390/biom9020065.

[25] K. Krollik, A. Lehmann, C. Wagner, J. Kaidas, H. Kubas, W. Weitschies, The effect of buffer species on biorelevant dissolution and precipitation assays – Comparison of phosphate and bicarbonate buffer, Eur. J. Pharm. Biopharm. 171 (2022) 90–101. https://doi.org/10.1016/j.ejpb.2021.09.009.

[26] D.F. Parsons, C. Carucci, A. Salis, Buffer-specific effects arise from ionic dispersion forces, Phys. Chem. Chem. Phys. (2022). https://doi.org/10.1039/d2cp00223j.

[27] K. Shortall, F. Otero, S. Bendl, T. Soulimane, E. Magner, Buffer on the Stability of the

Support, (2022). https://doi.org/10.1021/acs.langmuir.2c01630.

[28] O. Kravchenko, T.C. Sutherland, B. Heyne, Photobleaching of Erythrosine B in Aqueous Environment Investigation Beyond pH, Photochem. Photobiol. 98 (2022) 49–56. https://doi.org/10.1111/php.13396.

[29] M. Mura, C. Carucci, F.C. Marincola, M. Monduzzi, D.F. Parsons, A. Salis, Journal of Colloid and Interface Science The melting curves of calf thymus-DNA are buffer specific, J. Colloid Interface Sci. 630 (2023) 193–201. https://doi.org/10.1016/j.jcis.2022.10.018.

[30] A. Salis, M. Monduzzi, Not only pH. Specific buffer effects in biological systems, Curr. Opin. Colloid Interface Sci. 23 (2016). https://doi.org/10.1016/j.cocis.2016.04.004.

[31] A. Bhattacharya, R.J. Brea, H. Niederholtmeyer, N.K. Devaraj, A minimal biochemical route towards de novo formation of synthetic phospholipid membranes, Nat. Commun. 10 (2019) 1–8. https://doi.org/10.1038/s41467-018-08174-x.

[32] E. Leontidis, Investigations of the Hofmeister series and other specific ion effects using lipid model systems, Adv. Colloid Interface Sci. 243 (2017) 8–22. https://doi.org/10.1016/j.cis.2017.04.001.

[33] M.A. Johnson, S. Seifert, H.I. Petrache, A.C. Kimble-Hill, Phase coexistence in single-lipid membranes induced by buffering agents, Langmuir. 30 (2014) 9880–9885. https://doi.org/10.1021/la5018938.

[34] H. Bouvrais, L. Duelund, J.H. Ipsen, Buffers affect the bending rigidity of model lipid membranes, Langmuir. 30 (2014) 13–16. https://doi.org/10.1021/la403565f.

[35] A. Michanek, M. Björklund, T. Nylander, E. Sparr, SsRNA base pairing at a bilayer interface can be controlled by the acyl chain order, Soft Matter. 8 (2012) 10428–10438. https://doi.org/10.1039/c2sm06700e.

[36] D. Ye, X. Zuo, C. Fan, DNA Nanotechnology-Enabled Interfacial Engineering for Biosensor Development, Annu. Rev. Anal. Chem. 11 (2018) 171–195. https://doi.org/10.1146/annurev-anchem-061417-010007.

[37] Z. Zhang, Y. Yang, F. Pincet, M.C. Llaguno, C. Lin, Placing and shaping liposomes with reconfigurable DNA nanocages, Nat. Chem. 9 (2017) 653–659. https://doi.org/10.1038/nchem.2802.

[38] M. Langecker, V. Arnaut, T.G. Martin, J. List, S. Renner, M. Mayer, H. Dietz, F.C. Simmel, Synthetic lipid membrane channels formed by designed DNA nanostructures, Science (80-.). 338 (2012) 932–936. https://doi.org/10.1126/science.1225624.

[39] S.E. McNeil, Y. Perrie, Gene delivery using cationic liposomes, Expert Opin. Ther. Pat. 16 (2006) 1371–1382. https://doi.org/10.1517/13543776.16.10.1371.

[40] Nanomedicine and the COVID-19 vaccines, Nat. Nanotechnol. 15 (2020) 963. https://doi.org/10.1038/s41565-020-00820-0.

[41] P.L. Feigner, G.M. Ringold, Cationic liposome-mediated transfection, Nature. 337 (1989) 26–27.

[42] S. Bhattacharya, A. Bajaj, Advances in gene delivery through molecular design of cationic lipids, Chem. Commun. (2009) 4632–4656. https://doi.org/10.1039/b900666b.

[43] T. Montier, T. Benvegnu, P.-A. Jaffrès, J.-J. Yaouanc, P. Lehn, Progress in cationic lipid-mediated gene transfection: a series of bio-inspired lipids as an example., Curr. Gene Ther. 8

(2008) 296–312. https://doi.org/10.2174/156652308786070989.

[44] A. Ostróżka-Cieślik, B. Sarecka-Hujar, The Use of Nanotechnology in Modern Pharmacotherapy, Multifunct. Syst. Comb. Deliv. Biosensing Diagnostics. (2017) 139–158. https://doi.org/10.1016/b978-0-323-52725-5.00007-1.

[45] J.J. McManus, J.O. Rädler, K.A. Dawson, Does Calcium Turn a Zwitterionic Lipid Cationic?, J. Phys. Chem. B. 107 (2003) 9869–9875. https://doi.org/10.1021/jp034463d.

[46] D.H. Mengistu, K. Bohinc, S. May, Binding of DNA to zwitterionic lipid layers mediated by divalent cations, J. Phys. Chem. B. 113 (2009) 12277–12282. https://doi.org/10.1021/jp904986j.

[47] A.Y. Antipina, A.A. Gurtovenko, Molecular mechanism of calcium-induced adsorption of DNA on zwitterionic phospholipid membranes, J. Phys. Chem. B. 119 (2015) 6638–6645. https://doi.org/10.1021/acs.jpcb.5b01256.

[48] D. Morzy, R. Rubio-Sánchez, H. Joshi, A. Aksimentiev, L. Di Michele, U.F. Keyser, Cations Regulate Membrane Attachment and Functionality of DNA Nanostructures, J. Am. Chem. Soc. 143 (2021) 7358–7367. https://doi.org/10.1021/jacs.1c00166.

[49] D. McLoughlin, R. Dias, B. Lindman, M. Cardenas, T. Nylander, K. Dawson, M. Miguel, D. Langevin, Surface complexation of DNA with insoluble monolayers. Influence of divalent counterions, Langmuir. 21 (2005) 1900–1907. https://doi.org/10.1021/la047700s.

[50] C. Montis, Y. Gerelli, G. Fragneto, T. Nylander, P. Baglioni, D. Berti, Colloids and Surfaces B : Biointerfaces Nucleolipid bilayers : A quartz crystal microbalance and neutron reflectometry study, 137 (2016) 203–213.

[51] H.P. Wacklin, Current Opinion in Colloid & Interface Science Neutron re fl ection from supported lipid membranes, Curr. Opin. Colloid Interface Sci. 15 (2010) 445–454. https://doi.org/10.1016/j.cocis.2010.05.008.

[52] J.T. Andrews, K.E. Baker, J.T. Handloser, N. Bridges, A.A. Krone, P.J.N. Kett, Formation of Supported Lipid Bilayers (SLBs) from Buffers Containing Low Concentrations of Group i Chloride Salts, Langmuir. 37 (2021) 12819–12833. https://doi.org/10.1021/acs.langmuir.1c01707.

[53] A.P. Dabkowska, A. Michanek, L. Jaeger, M. Rabe, A. Chworos, F. Höök, T. Nylander, E. Sparr, Assembly of RNA nanostructures on supported lipid bilayers, Nanoscale. 7 (2015) 583–596. https://doi.org/10.1039/c4nr05968a.

[54] L. Schoenmaker, D. Witzigmann, J.A. Kulkarni, R. Verbeke, G. Kersten, W. Jiskoot, D.J.A. Crommelin, mRNA-lipid nanoparticle COVID-19 vaccines: Structure and stability, Int. J. Pharm. 601 (2021) 120586. https://doi.org/10.1016/j.ijpharm.2021.120586.

[55] J. Buck, P. Grossen, P.R. Cullis, J. Huwyler, D. Witzigmann, Lipid-Based DNA Therapeutics: Hallmarks of Non-Viral Gene Delivery, ACS Nano. 13 (2019) 3754–3782. https://doi.org/10.1021/acsnano.8b07858.

[56] Y. Ma, Y. Zhuang, X. Xie, C. Wang, F. Wang, D. Zhou, J. Zeng, L. Cai, The role of surface charge density in cationic liposome-promoted dendritic cell maturation and vaccine-induced immune responses, Nanoscale. 3 (2011) 2307. https://doi.org/10.1039/c1nr10166h.

[57] I.K. Vockenroth, C. Rossi, M.R. Shah, I. Köper, Formation of tethered bilayer lipid membranes probed by various surface sensitive techniques, Biointerphases. 4 (2009) 19–26. https://doi.org/10.1116/1.3122019.

[58] I. Koltover, T. Salditt, C.R. Safinya, Phase diagram, stability, and overcharging of lamellar cationic lipid- DNA self-assembled complexes, Biophys. J. 77 (1999) 915–924. https://doi.org/10.1016/S0006-3495(99)76942-0.

[59] M. V Voinova, M. Rodahl, M. Jonson, B. Kasemo, Viscoelastic Acoustic Response of Layered Polymer Films at Fluid-Solid Interfaces: Continuum Mechanics Approach, Phys. Scr. 59 (1999) 391–396. https://doi.org/10.1238/physica.regular.059a00391.

[60] H.G. Tompkins, WVASE32 Software Training Manual., (2006). www.jawoollam.com.

[61] B. Jachimska, K. Tokarczyk, M. Łapczyńska, A. Puciul-malinowska, S. Zapotoczny, Structure of bovine serum albumin adsorbed on silica investigated by Quartz Crystal Microbalance, Elsevier B.V. (2015). https://doi.org/10.1016/j.colsurfa.2015.10.033.

[62] C. Larsson, M. Rodahl, F. Höök, Characterization of DNA immobilization and subsequent hybridization on a 2D arrangement of streptavidin on a biotin-modified lipid bilayer supported on SiO2, Anal. Chem. 75 (2003) 5080–5087. https://doi.org/10.1021/ac034269n.

[63] F. Höök, B. Kasemo, T. Nylander, C. Fant, K. Sott, H. Elwing, Variations in coupled water, viscoelastic properties, and film thickness of a Mefp-1 protein film during adsorption and cross-linking: A quartz crystal microbalance with dissipation monitoring, ellipsometry, and surface plasmon resonance study, Anal. Chem. 73 (2001) 5796–5804. https://doi.org/10.1021/ac0106501.

[64] G. Pinto, S. Dante, S. Maria, C. Rotondi, P. Canepa, O. Cavalleri, M. Canepa, Spectroscopic Ellipsometry Investigation of a Sensing Functional Interface : DNA SAMs Hybridization, Adv. Mater. Interfaces. 9 (2022) 2200364. https://doi.org/10.1002/admi.202200364.

[65] R. Kou, J. Zhang, T. Wang, G. Liu, Interactions between Polyelectrolyte Brushes and Hofmeister Ions: Chaotropes versus Kosmotropes, Langmuir. 31 (2015) 10461–10468. https://doi.org/10.1021/acs.langmuir.5b02698.

[66] K.D. Collins, Ions from the Hofmeister series and osmolytes: Effects on proteins in solution and in the crystallization process, Methods. 34 (2004) 300–311. https://doi.org/10.1016/j.ymeth.2004.03.021.

[67] B.W. Ninham, V. Yaminsky, Ion binding and ion specificity: The Hofmeister effect and Onsager and Lifshitz theories, Langmuir. 13 (1997) 2097–2108. https://doi.org/10.1021/la960974y.

[68] B.W. Ninham, P. Lo Nostro, Molecular Forces and Self Assembly : In Colloid, Nano Sciences and Biology, Cambridge University Press, Cambridge, 2010.

[69] D.W. Smith, Ionic Enthalpies, J. Chem. Educ. 1 (1977) 1–3.

[70] L. Medda, C. Carucci, D.F. Parsons, B.W. Ninham, M. Monduzzi, A. Salis, Specific cation effects on hemoglobin aggregation below and at physiological salt concentration., Langmuir. 29 (2013) 15350–15358. https://doi.org/10.1021/la404249n.

[71] L. Medda, M. Monduzzi, A. Salis, The molecular motion of bovine serum albumin under physiological conditions is ion specific, Chem. Commun. 51 (2015) 6663–6666. https://doi.org/10.1039/c5cc01538c.

[72] C. Carucci, F. Raccis, A. Salis, E. Magner, Specific ion effects on the enzymatic activity of alcohol dehydrogenase from Saccharomyces cerevisiae, Phys. Chem. Chem. Phys. 22 (2020) 6749–6754. https://doi.org/10.1039/C9CP06800G.

[73] D.F. Parsons, A. Salis, The impact of the competitive adsorption of ions at surface sites on surface free energies and surface forces, J. Chem. Phys. 142 (2015) 134707. https://doi.org/10.1063/1.4916519.

[74] D.F. Parsons, T.T. Duignan, A. Salis, D.F. Parsons, Cation effects on haemoglobin aggregation : balance of chemisorption against physisorption of ions, Interface Focus. 7 (2017) 20160137.

[75] D.F. Parsons, A. Salis, A thermodynamic correction to the theory of competitive chemisorption of ions at surface sites with nonelectrostatic physisorption, J. Chem. Phys. 151 (2019) 024701. https://doi.org/10.1063/1.5096237.

[76] F. Cugia, S. Sedda, F. Pitzalis, D.F. Parsons, M. Monduzzi, A. Salis, Are specific buffer effects the new frontier of Hofmeister phenomena? Insights from lysozyme adsorption on ordered mesoporous silica, RSC Adv. 6 (2016) 94617–94621. https://doi.org/10.1039/C6RA17356J.

[77] M.M. Koerner, L.A. Palacio, J.W. Wright, K.S. Schweitzer, B.D. Ray, H.I. Petrache, Electrodynamics of lipid membrane interactions in the presence of zwitterionic buffers, Biophys. J. 101 (2011) 362–369. https://doi.org/10.1016/j.bpj.2011.05.062.